Mon. Not. R. Astron. Soc. **272**, 49–60 (1995)

The spectrum of the planetary nebula NGC 6886

Siek Hyung,* Charles D. Keyes*†‡ and Lawrence H. Aller*†
Astronomy Department, University of California, Los Angeles, CA 90024, USA

Accepted 1994 July 30. Received 1994 May 20; in original form 1994 February 24

ABSTRACT

The relatively young, high-excitation planetary nebula (PN) NGC 6886 shows a remarkable variety of lines from both high- and low-excitation stages, i.e., from N^0 to N^{4+}, and as a result it provides unique opportunities for detailed studies of physical processes, using a theoretical model. By combining Hamilton echelle observations with UV data secured with the *International Ultraviolet Explorer* (*IUE*) satellite, and with available IR data, we can obtain improved diagnostics and elemental abundances which should supply insights into nucleogenesis processes and properties of the progenitor star. Improved theoretical nebular models are employed. The chemical composition of this high-excitation PN is found from ionic concentrations, and also from a theoretical model. Except for Ne, Si and Cl, the agreement between the abundances calculated using the two methods is generally remarkably good. The C/H ratio is enhanced by about 15–20 per cent above the solar value, but the N/H and Ne/H, and probably Si/H ratios, are close to those of the Sun. The other 'metal'/H ratios and the He/H ratio seem to be lower than in the Sun, and O is depleted. If pronounced T_ε fluctuations are assumed, we can raise the abundances of O, S, Cl and Ar to approximately solar values, but then C, N and Ne are substantially enhanced. Since the distance is poorly determined, it is difficult to establish evolutionary parameters.

Key words: ISM: abundances – planetary nebulae: general – planetary nebulae: individual: NGC 6886 – ultraviolet: ISM.

1 INTRODUCTION

Since planetary nebulae (PNe) are the ejecta of highly evolved stars, their chemical compositions supply crucial information in the study of stellar evolution and nucleogenesis calculations. N-rich objects are presumed to originate from objects where the CNO cycle ran to completion, the C-rich objects are those that burned He to C, while O-rich objects presumably display the chemistry of the progenitor star, although in some objects, e.g. NGC 6537, O can be depleted by 'hot bottom' burning. Given the nebular distance, our modelling procedures permit us to set constraints on the temperature and luminosity of the central star (PNN), and presumably on its evolutionary status. Accurate nebular chemical compositions should help us to assess nucleogenesis scenarios which depend on the progenitor star mass and its own initial chemical composition, which presumably reflects that of the contemporary interstellar medium from which it was formed.

NGC 6886 was chosen for our investigation, because it appears to be a relatively young, high-excitation PN with a rich spectrum, so that we can obtain abundance estimates for an especially wide variety of elements both by the ionization correction factor (ICF) method and by modelling. We would like to establish the mass and luminosity of the central star and thus define the evolutionary status of this object, but we are frustrated by our lack of an accurate knowledge of its distance. The progenitor star appears to have had approximately solar C, N and Ne abundances with depleted O abundance or enhanced C, N and Ne abundances and possibly approximately normal abundances of O, S, Cl and Ar – if pronounced T_ε fluctuations exist.

Table 1 summarizes the pertinent data for NGC 6886. Aller & Czyzak (1979) secured spectral data from 3132 to

* Electronic mail (SPAN):bonnie::hyung;stscic::keys;bonnie::aller.
†Guest observer with the *IUE* satellite, which is sponsored and operated by the National Aeronautics and Space Administration, by the European Space Agency, and by the Particle Physics and Astronomy Research Council of the UK.
‡Present address: Space Telescope Science Institute, Mail Stop: SIB/SPD 3700 San Martin Drive, Baltimore, MD 21218, USA.

Table 1. Some basic data for NGC 6886 (PK 60 − 07°2).

$\alpha = 20^h\ 12^m\ 42.^s9$, $\delta = +\ 19°\ 59'\ 22''$ (2000)

Diameter = 5.5″

log F(Hβ) = −11.28 & −11.31 (Heap et al. 1991 & Cahn et al. 1992)

V(exp) = 20.3 km s^{-1} [NeIII], & 22.7 km s^{-1} [OII] (Sabbadin 1984)

V(exp) = 20.0 km s^{-1} [OIII], & 25.5 km s^{-1} [NII] (Weinberger 1989)

V(exp) ≃ 22.8 km s^{-1} HI (Taylor et al. 1990)

Radius = 3.7″, excitation class = 8 (Aller 1974; Pottasch 1984)

Central star: V magnitude = 18.76

Distance = 2000 pc (Pottasch 1983)

See Catalogue of Planetary Nebulae (Acker et al. 1992) for additional data and a complete set of references.

8577 Å with an image tube scanner (ITS) at Lick Observatory. In the near-UV, λ3100–3900 Å, Likkel & Aller (1986) obtained improved ITS data for a study of the Bowen fluorescent line; we are indebted to Dr Likkel, who measured these scans completely. The relatively low spectral resolution of the ITS was insufficient to separate [O II]λ3726/λ3729, [Ar IV]λ4711/He Iλ4713, [S III]λ6312/He IIλ6311 and [N I]λ5200/λ5198. The high resolution attainable with the Hamilton echelle spectrograph gives good separations for these lines, so the nebular diagnostics and plasma conditions in various ionic stages can be evaluated better. In Section 2, we describe the UV and optical observations, and tabulate line identifications and intensities on the scale $F(\mathrm{H}\beta) = 100$. We also give the extinction-corrected line intensities on the scale $I(\mathrm{H}\beta) = 100$. In Section 3, we discuss the physical state of the PN with plasma diagnostics, and obtain fractional ionic abundances from collisionally excited lines. The diagnostics of [N I], [Ar V], [Ar IV], [S III] and [Cl IV]λ5323/(λ7530 + λ8045), which were not available from the ITS data, are now obtainable with Hamilton echelle spectrograph data. In Section 4, we present a photoionization model, from which we derive for each element the appropriate ICF, with the aid of which we can estimate the nebular chemical composition. We conclude our paper with some remarks and comments on the possible evolutionary status of NGC 6886.

2 THE OBSERVATIONS

2.1 The UV spectrum

Observations of NGC 6886 were secured in the low-dispersion mode of the *IUE* on 1988 November 25–26. All data were taken with the large entrance aperture, 10 × 23 arcsec^2, of the *IUE* cameras, with the central star centred in the aperture. These data supplement earlier observations secured in 1979.

Table 2(a) summarizes the UV spectrum as measured from the low-dispersion spectra, SWP34816 (420 min) and LWP14546 (410 min), supplemented with earlier data, SWP5214 (45 min) and LWR4509 (60 min). Fluxes of weak or uncertain lines are denoted by (?). All observed fluxes in column (3) are in units of 10^{-14} erg cm^{-2} s^{-1}. We tried to determine the interstellar extinction from the observed $F(1640)$ and an integrated $F(4686)$ [and $F(\mathrm{H}\beta)$] quoted from the various sources, i.e., Aller & Keyes (1981) and Heap et al. (1991); the result is $C \simeq 0.973$ from $F(1640)/F(4686)$, assuming $T_e = 12\,600$ K and $N_e = 7000$ cm^{-3} (Aller & Czyzak 1979). We applied $C = 0.973$ to the UV data. Column (4) gives the adopted value of the extinction function, k_λ, at each wavelength from Seaton (1979). Column (5) gives the intensities, corrected to the scale $I(H\beta) = 100$ as described below. Lines of the following ions are observed in the *IUE* nebular spectrum: He I, He II, C II, C II], C III], C IV, [N I], N III], N IV, N IV], N V, [O II], O III, O III], [O III], O V], [Ne III], [Ne IV], [Ne V], Si II, Si III], [Ar IV], [Ar V], Mg II and [Mg V].

Data for the near-UV, based largely on ITS scans, are given in Table 2(b). Successive columns give wavelength, identification, flux relative to $F(\mathrm{H}\beta) = 100$, quality, k_λ, and reddening-corrected intensity to scale $I(\mathrm{H}\beta) = 100$. This table is compiled from Aller & Czyzak (1979), supplemented by new ITS scans secured by Likkel & Aller (1986). They used, typically, a 2 × 10 arcsec^2 slot with the long dimension perpendicular to the horizon.

2.2 The optical region

All the optical-region spectroscopic measurements utilized here were secured with the Hamilton echelle spectrograph at the Shane 3-m telescope at the Lick Observatory. We measured lines from 3650 to 10 050 Å on 1993 August 8–9, centring on the nebular nucleus. The adopted slot size of the spectrograph, 640 μm (≃ 1.2 arcsec) × 4.0 arcsec is somewhat smaller than the nebula.

The echelle pattern fans out as the wavelength increases. Also, since the dispersion produced by the prism placed in the beam to separate the orders decreases sharply from the violet to the red, the individual segments of the spectrum fall closer together with increasing wavelength. Use of the CCD (charge coupled device) 800 × 800 pixel chip (which we

Table 2. (a) Ultraviolet line fluxes and intensities normalized to $I(\mathrm{H}\beta) = 100$ and corrected for interstellar extinction ($C = 0.973$).

$\lambda_{obs'd}$ (1)	Element (2)	F(IUE)/E-14 (3)	k_λ (4)	I(IUE) (5)	Notes (6)
1239/43	N V	4.9	1.641	64.2	
1403-13	O IV]	11.0	1.308	68.2	
1487	N IV]	9.6	1.231	49.9	
1503.9	N IV]	8.2	1.220	41.7	
1548/50	C IV	12.8	1.185	603	
1575	[Ne V]?	8.3	1.169	37.7	
1603.7	[Ne IV]	8.7	1.151	38.1	
1640	He II	68.8	1.138	292	
1660/66	O III]	9.9±2.7	1.130	41.4	
1679	?	4.4?	1.127	18.2	
1718	N IV?	13?	1.120	53.0	
1747-52	N III]	13.0	1.121	53.0	
1760.8	C II?	8.0	1.126	33.0	
1817	Si II,[Ne III]	2.5	1.143	10.8	
1883/92	Si III]	8.1	1.208	40.1(32[1])	
1907/09	C III]	180±12	1.228	93.4	
2253	He II	1.384	1.546	14.6	
2323	C II],[O III]	28.2±0.1	1.353	193.3	
2423/25	[Ne IV]	36.7±2.0	1.122	150.0	
2470	[O II]	12.3±1.0	1.027	40.7	
2734	He II	8.68	0.701	13.8	
2784/86	[Mg V],[Ar V]	> 7.0	0.660	10.2	S
2796/2803	Mg II	19.2±4?	0.647	27.1	
2818		> 2	0.637	2.76	S
2836.6	O III,C II	10.0	0.629	13.5	
2858.8	[Ar IV]	> 2.3	0.605	2.96	S
2870.1	[Ar IV]	1.53	0.598	1.93	
2907.9		1.8	0.574	2.16	
2930	[Mg V],Mg II	4.34	0.560	5.03	
2946.1	He I	2.4	0.550	2.73	
3025.4	O III	6.3±1.8	0.507	6.5	
3044.2	O III	15.6±1.5	0.496	15.6	

[1]Average. S: saturated.

Table 2. (b) Near-UV line fluxes based on ITS data.

$\lambda_{obs'd}$ (1)	Element (2)	F(ITS) (3)	Q (4)	k_λ (5)	I_c (6)
3133	OIII	25:	D	0.455	83:
3188	HeI	0.87:	C-	0.432	2.8:
3202	HeII	4.8	B	0.426	14.8
3241	[NaIV]	0.21	D	0.410	0.92
3261	OIII	0.2	E	0.403	0.5:
3287	—	0.29	D	0.390	0.8
3299	OIII	0.8	B	0.388	2.23
3312	OIII	2.2	A	0.384	6.16
3318	[FeIII]	0.49	C?	0.382	1.35
3328		0.13	E	0.377	0.3:
3341	OIII	3.6	A	0.373	9.67
3346	[NeV]	11.0	A	0.372	29.5
3362	[NaIV]	0.16	D	0.366	0.42
3381	OIV	0.23	D	0.360	0.60
3385	OIV	0.2:	E	0.358	0.5:
3397	OIV	0.11	D	0.354	0.28
3406	OIII	0.21	D	0.351	0.53
3412	OIV	0.37	D	0.349	0.90
3415	OIII	0.27		0.348	0.7:
3426	[NeV]	33.8	A	0.345	84.3
3428	OIII	1.6		0.344	4.0
3444	OIII	8.4	A	0.339	20.6
3466		0.09	D-	0.330	0.2:
3480		0.15	D-	0.320	0.35:
3513	HeI	0.17	D-	0.320	0.4:
3530	HeI	0.08	D-	0.312	0.18:
3554	HeI	0.14	D-	0.305	0.32:
3587	HeI	0.16	D-	0.296	0.35
3613	HeI	0.12	D	0.289	0.26
3634	HeI	0.18		0.283	0.38

:Estimated uncertainty ≥ 50 per cent.

found to be most satisfactory for our purposes) required six different chip settings, since the area of the chip was much smaller than that of the echelle pattern. The six positions are: setting #1 for the region shortward of 4600 Å; setting #3 for the region from 6000 to 4200 Å; setting #7 covers much of the region from 7000 to 4400 Å, and allows us to tie Hα, [O III] and Hβ together on one exposure; finally, the deep-red $5300 < \lambda < 10\,200$ Å is covered by three settings, #4, #5 and #6. The integration time varies for each setting; short exposures of 5 min are needed for the strong lines in each setting. To register the weaker lines we need longer exposures, usually 50 min except for #1 (90 min) and #5 (60 min). Fig. 1 shows one of the frames centred on the red region of the spectrum. Considerable overlap between different chip settings enables us to combine intensities more effectively. For each of the six required positions, we must obtain measurements of the Th–Ar comparison arc, the 'flat-field', and a comparison star. Hyung (1994) describes the necessary procedures in detail.

Table 3 summarizes the optical-region line intensity data for NGC 6886. The first column gives the observed λ corrected for the radial velocity, $V_{\mathrm{rad}} = -33.04$ km s^{-1}, of the nebula with respect to the observer at the time of observation; column (2) gives the laboratory wavelength of the line identified in column (3), while column (4) lists the multiplet number, on the system of Moore (1972).

In order to determine interstellar extinction, we can compare the observed hydrogen recombination flux ratios with the theoretical ratios under appropriate nebular conditions. We derived the extinction coefficient, $C = \log I(\mathrm{H}\beta)/F(\beta)$, using (a) Balmer line ratios such as $F(\mathrm{H}\alpha)/F(\mathrm{H}\beta)$, $F(\mathrm{H}\gamma)/F(\mathrm{H}\beta)$, and (b) the Paschen to Balmer line ratios, $F(\mathrm{P}n)/F(\mathrm{H}\beta)$, or (c) $F(\mathrm{P}n)/F(\mathrm{H}n)$s. The theoretical intrinsic values were taken from Hummer & Storey (1987). Apparently, the intrinsic ratios of recombination-line fluxes are somewhat sensitive to the density and temperature over the range with which we are concerned (see diagnostics in Section 3). For a nebular condition where $T_e = 13\,000$ K, $N_e = 12\,000$ cm^{-3} (the value used in some earlier studies, i.e., Rowlands et al. 1989), we obtained (a) $C = 1.49 \pm 0.31$ [$C = 1.02$ from $F(\mathrm{H}\alpha)/F(\mathrm{H}\beta)$], (b) $C = 0.33 \pm 0.12$, and (c) $C = 0.99 \pm 0.16$, while for $T_e = 12\,000$ K, $N_e = 7000$ cm^{-3} (Che & Köppen 1983 and the final model in Section 4), more consistent values of (a) $C = 0.93 \pm 0.20$ [$C = 0.90$ from $F(\mathrm{H}\alpha)/F(\mathrm{H}\beta)$], (b) $C = 0.79 \pm 0.09$, and (c) $C = 0.88 \pm 0.15$ are obtained. We have adopted $C = 0.90$ from the latter for application to the Hamilton spectrograph data compiled in Table 3. This extinction coefficient differs slightly from the value applied in Section 2.1 to the UV data, $C = 0.973$, and more substantially from that assumed for analysis of the ITS data by Aller & Czyzak (1979), $C \sim 1.08$, probably due to the differing segments of the nebula sampled by the apertures of the various spectrographs and differences in adopted response functions. The interstellar extinction coefficient, k_λ, as derived from equations given by Seaton (1979), is given in column (5). Column (6) gives the line intensity $I(\mathrm{Ham})$ relative to $I(\mathrm{H}\beta) = 100$ corrected for interstellar extinction, $C = 0.90$. The uncorrected flux $F(\mathrm{Ham})$ relative to $F(\mathrm{H}\beta) = 100$ is given in column (7), and the formal root mean square (RMS) percentage error, as deduced from internal agreement of measurements made with different chip settings (when two or more independent measurements

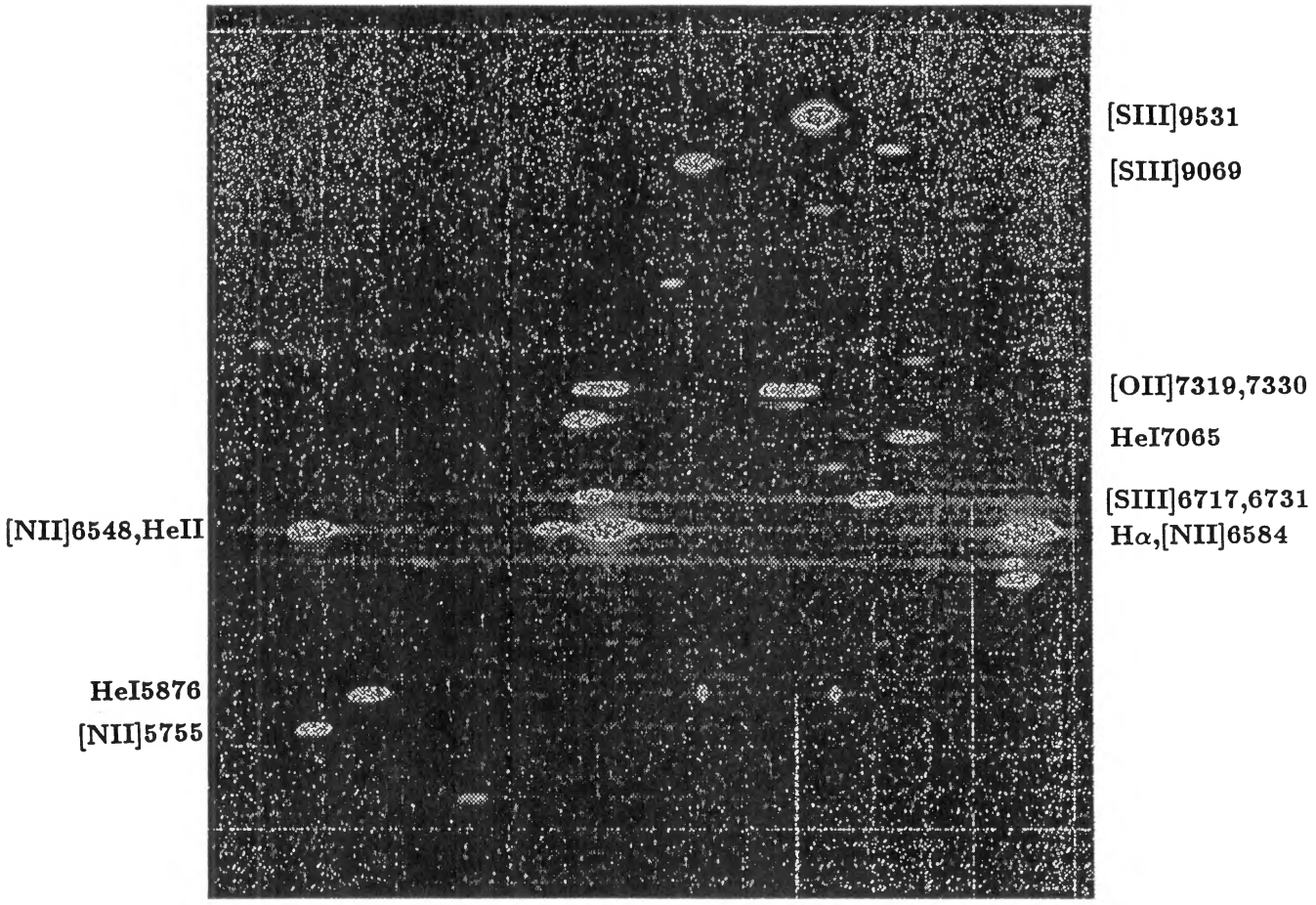

Figure 1. An echellogram of NGC 6886. This exposure at chip setting #125 covers much of region λλ5250–10 510 Å: 60-min exposure, 1993 August 9.

are available), is in column (8). The actual errors are larger; see the discussion in Hyung (1994). We used the notation 'Ham' to denote lines measured with the Hamilton spectrograph. Lines of the following ions are observed with the Hamilton echelle: H, He I, He II, [C I], C II, C III, C IV, [N I], N II, [N II], N III, [N III], N IV, [O I], O II, [O II], O III, [O III], O IV, [Ne III], [Ne IV], Mg I, [Mg I], Si II, [S I], S II, [S II], [S III], [S IV], [Cl II], [Cl III], [Cl IV], [Ca V], Ar II, [Ar III], [Ar IV], [Ar V], [Fe III], [Fe V], [Fe VI] and [K IV]. [S IV] has been observed in the IR by Beck et al. (1981) and others. [Na IV] has been observed in the near-UV.

3 DIAGNOSTIC DIAGRAM

Fig. 2 shows the diagnostic diagram based on Hamilton data. Part of the scatter for the same ionic stage is due to observational error. Since the auroral lines of [Ar V]4625 and [Cl IV]5323 have intensities of 0.14 and 0.10 respectively, which are near the lower limit of measurability, we can measure no meaningful $T(Ar^{+4})$ or $T(Cl^{+3})$. A small observational error in critical spectral lines can result in a large scatter for derived diagnostics; e.g., for ~6 per cent errors in [O III] lines, $\Delta T = \pm 1500$ K, and, for ~10 per cent errors in [Cl III], $\Delta \log N_\varepsilon = \pm 0.25$. The average electron temperature is ~12 000 K from [O III] and [Ar III]. This value is lower than that suggested by earlier studies (14 000 K). The nebular transitions of [S III] are affected by atmospheric absorption, so $T([S III])$ is systematically too high. [N II] appears to originate in a cooler zone, $T_\varepsilon \sim 10\,000$ K. The diagnostics from auroral/nebular-type transition ratios in [S II], [O II] and [Ar IV], denoted as [O II]−, [S II]− and [Ar IV]−, do not give results in satisfactory accord with those indicated by the nebular line ratios. The population of the ^2P level is systematically too large. The nebular line ratios in [S II] and [O II] imply a very low electron density of $N_\varepsilon \sim 2000$ cm^{-3}, while the auroral/nebular lines suggest $N_\varepsilon \sim 10\,000$ cm^{-3}. Possibly there may exist zones of greatly differing density and temperature, or possibly there still remain unresolved errors in the atomic parameters.

The diagnostics available from earlier ITS and photographic data (Aller & Czyzak 1979) are presented in Fig. 3. Because of the low resolution, no diagnostics for [N I], [Ar V], [Ar IV], [S III] and [Cl IV]λ5323/(λ7530+λ8045) can be found from ITS data. For the visual and near-IR, Aller & Czyzak had to rely on ITS results, whilst for the blue region high-resolution photographic measurements were available. In the blue-wavelength region, the Hamilton echelle detector

Table 3. Optical-region line intensities in NGC 6886.

$\lambda_{obs'd}$ (1)	λ_{lab} (2)	Element (3)	Mult. (4)	k_λ (5)	I(Ham) (6)	F(Ham) (7)	RMS (8)
3691.55	3691.56	H I	H18	0.267	2.13	1.22	
3697.38	3697.15	H I	H17	0.265	1.48	0.86	
3702.07		?		0.264	1.25	0.72	
3704.74	3705.02	He I	(25)	0.271	1.35	0.77	
3711.94	3711.97	H I	H15	0.269	2.17	1.24	
	3721.94	H I	H14				
3721.88	3721.83	[S III]	(2F)	0.267	2.91	1.67	
3726.05	3726.03	[O II]	(1F)	0.266	61.38	35.40	
3728.78	3728.82	[O II]	(1F)	0.265	40.03	23.12	
3734.45	3734.37	H I	H13	0.263	2.33	1.35	
3750.16	3750.15	H I	H12	0.259	2.01	1.17	
3754.60	3754.67	O III	(2)	0.258	1.08	0.64	
3759.89	3759.81	O III	(2)	0.256	2.95	1.73	
3770.81	3770.63	H I	H11	0.253	3.50	2.07	
3797.95	3797.90	H I	H10	0.246	2.91	1.75	
3819.41	3819.61	He I	(22)	0.241	1.81	1.10	
3835.36	3835.39	H I	H9	0.236	7.74	4.74	
3868.77	3868.71	[Ne III]	(1F)	0.228	146.93	91.62	1.5%
	3889.05	H I	H8				
3888.83	3888.65	He I	(2)	0.223	27.33	17.22	
3923.46	3923.48	He II	(4)	0.214	0.71	0.45	
3964.57	3964.73	He I	(5)	0.204	0.50	0.33	
3967.42	3967.41	[Ne III]	(1F)	0.203	51.54	33.81	10.6%
3970.03	3970.07	H I	Hϵ	0.203	20.87	13.71	
4026.10	4026.36	He I	(18)	0.189	2.46	1.66	
4047.09		?		0.185	0.46	0.31	
4068.68	4068.60	[S II]	(1F)	0.180	4.86	3.35	
4076.29	4076.35	[S II]	(1F)	0.178	1.73	1.20	
4097.40	4097.31	N III	(1)	0.173	1.35	0.94	
4100.10	4100.04	He II	(3)	0.172	0.61	0.43	
4101.74	4101.76	H I	Hδ	0.172	27.98	19.59	
4103.37	4103.37	N III	(1)	0.172	0.65	0.46	
4120.87	4120.81	He I	(16)	0.168	0.43	0.30	
4199.80	4199.83	He II	(3)	0.152	0.82	0.60	
4227.56	4227.44	[Fe V]		0.147	0.15	0.11	
4267.11	4267.18	C II	(6)	0.141	0.43	0.32	
4338.69	4338.67	He II		0.129	1.11	0.85	16.1%
4340.47	4340.47	H I	Hγ	0.129	48.19	36.90	2.8%
4363.19	4363.21	[O III]	(2F)	0.124	18.42	14.26	17.8%
4387.92	4387.93	He I	(51)	0.117	0.37	0.29	

Table 3 – *continued*

$\lambda_{obs'd}$ (1)	λ_{lab} (2)	Element (3)	Mult. (4)	k_λ (5)	I(Ham) (6)	F(Ham) (7)	RMS (8)
4471.51	4471.50	He I	(14)	0.095	3.22	2.65	16.1%
	4510.93	[K IV]?	(2F)				
4510.81	4510.92	N III	(3)	0.085	0.19	0.16	
4541.62	4541.59	He II		0.077	1.43	1.22	3.9%
4562.53	4562?	[Mg I]?	(1)	0.072	0.23	0.20	
4571.15	4571.00	Mg I	(1)	0.070	0.90	0.78	16.5%
4606.51	4506?	N IV?,[FeIII]	(3F)	0.061	0.14	0.12	25.7%
4625.52	4625?	[Ar V]?	(2F)	0.056	0.14	0.12	
4632.15	4631.9?	O IV?		0.055	0.20	0.18	23.1%
4634.13	4634.16	N III	(2)	0.054	1.51	1.35	4.7%
4640.65	4640.64	N III	(2)	0.053	2.91	2.61	2.6%
4641.90	4641.90	N III	(2)	0.052	0.41	0.37	8.5%
4647.50	4647.40	C III	(1)	0.051	0.41	0.37	29.3%
4649.03	4649.14	O II	(1)	0.051	0.20	0.18	5.9%
4650.51	4650.84	O II	(1)	0.050	0.20	0.18	31.5%
4651.68	4651.35	C III	(1)	0.050	0.11	0.10	
4657.60	4658.10	[Fe III]	(3F)	0.049	0.14	0.13	
4658.48	4658.64	C IV	(3F)	0.049	0.31	0.28	13.8%
4661.90	4661.64	O II	(1)	0.048	0.14	0.13	
4685.74	4685.68	He II	(1)	0.042	46.22	42.36	3.5%
4711.36	4711.34	[Ar IV]	(1F)	0.036	5.92	5.50	5.1%
4713.08	4713.14	He I	(12)	0.036	0.80	0.74	11.0%
4714.25	4714.25	[Ne IV]	(1F)	0.035	0.73	0.68	10.5%
4715.71	4715.61	[Ne IV]	(1F)	0.035	0.31	0.29	12.2%
4724.14	4724.15	[Ne IV]	(1F)	0.033	0.65	0.61	16.2%
4725.57	4725.62	[Ne IV]	(1F)	0.033	0.54	0.51	12.8%
4740.22	4740.20	[Ar IV]	(1F)	0.029	7.66	7.21	6.2%
4859.33	4859.32	He II	(2)	0.000	2.09	2.09	12.4%
4861.31	4861.33	H I	Hβ	0.000	100.00	100.00	8.4%
4921.96	4921.93	He I	(48)	-0.015	1.13	1.16	12.6%
4930.97	4931.30	[O III]	(1F)	-0.017	0.27	0.28	
	4958.90	[Fe III]	(2F)				
4958.87	4958.92	[O III]	(1F)	-0.023	537.24	563.64	5.3%
4987.31	4987.30	[Fe III]	(2F)	-0.030	0.14	0.15	
4996.21		?		-0.032	0.53	0.57	
5006.86	5006.84	[O III]	(1F)	-0.034	1715.19	1840.77	
5015.69	5015.68	He I	(4)	-0.036	1.50	1.62	
5017.46	5017.63	Ar II	(13)	-0.036	0.44	0.47	
5031.30		?		-0.039	0.10	0.10	
5041.15	5041.06	Si II	(2)	-0.041	0.19	0.21	

Table 3 – *continued*

$\lambda_{obs'd}$ (1)	λ_{lab} (2)	Element (3)	Mult. (4)	k_λ (5)	I(Ham) (6)	F(Ham) (7)	RMS (8)
5047.66	5047.74	He I	(47)	-0.043	0.20	0.22	
5056.29	5056.35	Si II	(5)	-0.045	0.42	0.46	
	5146.06	O I?	(28)				
5145.92	5145.80	[Fe VI]	(2F)	-0.063	0.12	0.14	
5176.19	5176.28	Ar II	(37)	-0.070	0.10	0.11	
5191.79	5191.80	[Ar III]	(3F)	-0.073	0.28	0.32	5.7%
5197.93	5197.90	[N I]	(1F)	-0.074	0.67	0.78	
5200.27	5200.26	[N I]	(1F)	-0.074	0.41	0.48	
5309.22	5309.20	[Ca V]	(1F)	-0.097	0.18	0.22	
5323.09	5323.30	[Cl IV]	(3F)	-0.100	0.10	0.13	
5335.21	5335?	[Fe VI]	(1F)	-0.102	0.13	0.17	
5345.97	5345.67	S II	(38)	-0.105	0.08	0.10	
5411.57	5411.52	He II	(2)	-0.118	3.14	4.01	12.4%
5517.69	5517.71	[Cl III]	(1F)	-0.139	0.43	0.57	15.7%
5537.82	5537.88	[Cl III]	(1F)	-0.143	1.09	1.47	5.0%
5576.87	5577.34	[O I] atm?	(3F)	-0.152	0.73	1.00	
5577.51	5577.34	[O I]	(3F)	-0.152	0.26	0.36	14.7%
5592.26	5592.37	O III	(5)	-0.155	0.16	0.22	11.8%
5754.54	5754.64	[N II]	(3F)	-0.191	4.49	6.67	7.2%
5801.39	5801.51	C IV	(1)	-0.201	0.16	0.24	26.5%
5812.05	5812.14	C IV	(1)	-0.203	0.12	0.18	0.5%
5867.64	5867.82	HeII	(29)	-0.214	0.09	0.14	
5875.54	5875.67	He I	(11)	-0.216	9.41	14.72	14.2%
	5932.20	He II	(25)				
5931.71	5931.79	N II	(28)	-0.226	0.06	0.09	
5953.11	5953.10	He II	(24)	-0.229	0.06	0.10	
5977.02	5977.00	He II	(23)	-0.233	0.07	0.12	
6004.75	6004.80	He II	(22)	-0.238	0.07	0.12	4.2%
6036.95	6037.20	He II	(21)	-0.243	0.03	0.05	
6074.27	6074.30	He II	(20)	-0.250	0.12	0.20	16.6%
6086.83		[CaV],[FeVI]	(1F)	-0.252	0.14	0.23	2.2%
6101.77	6101.80	[K IV]	(1F)	-0.254	0.31	0.53	8.2%
6104.24	6104?	[K IV]??		-0.254	0.09	0.14	
6118.15	6118.20	He II	(8)	-0.257	0.11	0.19	
6170.77	6170.70	He II	(18)	-0.265	0.13	0.22	9.1%
6231.76	6230?	He I?		-0.274	0.13	0.24	71.1%
6233.87	6233.80	He II	(17)	-0.275	0.12	0.20	25.6%
6300.37	6300.30	[O I]	(1F)	-0.285	10.76	19.41	18.3%
6310.76	6310	He II?	(16)	-0.286	0.16	0.29	33.3%
6312.08	6312.10	[S III]	(3F)	-0.287	2.74	4.97	6.8%

Table 3 – *continued*

$\lambda_{obs'd}$ (1)	λ_{lab} (2)	Element (3)	Mult. (4)	k_λ (5)	I(Ham) (6)	F(Ham) (7)	RMS (8)
6347.44	6347.09	Si II	(2)	-0.292	0.05	0.10	
6363.89	6363.78	[O I]	(1F)	-0.294	4.25	7.82	4.3%
6406.37	6406.50	He II	(15)	-0.301	0.26	0.49	14.2%
6435.11	6435.10	[Ar V]	(1F)	-0.305	1.11	2.09	9.5%
6527.13		?		-0.318	0.26	0.50	11.7%
6544.27		?		-0.320	0.18	0.35	
6548.02	6548.03	[N II]	(1F)	-0.321	71.02	138.04	2.1%
6560.12	6560.00	He II	(6)	-0.322	6.25	12.19	5.0%
6562.80	6562.82	H I	Hα	-0.323	282.17	550.81	2.2%
6578.32	6578.03	C II	(2)	-0.325	0.41	0.80	
6583.54	6583.41	[N II]	(1F)	-0.326	215.24	422.67	6.2%
6678.24	6678.15	He I	(46)	-0.338	2.74	5.52	0.7%
6683.21	6683.20	He II	(7)	-0.339	0.29	0.59	5.5%
6716.47	6716.47	[S II]	(2F)	-0.343	5.92	12.05	2.7%
6730.79	6730.85	[S II]	(2F)	-0.345	12.24	25.00	2.0%
6794.87		?		-0.352	0.06	0.13	
6890.96	6890.88	He II	(7)	-0.363	0.35	0.75	
7005.67	7005.70	[Ar V]	(1F)	-0.376	1.89	4.12	8.5%
7065.25	7065.28	He I	(10)	-0.383	5.19	11.48	12.9%
7135.69	7135.78	[Ar III]	(1F)	-0.391	26.33	59.16	0.5%
7170.62	7170.62	[Ar IV]	(2F)	-0.394	0.26	0.59	12.0%
7177.43	7177.50	He II	(6)	-0.395	0.34	0.76	12.3%
7237.39	7237.54	[Ar IV]	(2F)	-0.401	0.43	0.99	
7262.97	7262.70	[Ar IV]	(2F)	-0.404	0.20	0.45	5.5%
7281.31	7281.35	He I	(45)	-0.406	0.63	1.47	12.0%
7319.88	7319.65	[O II]	(2F)	-0.410	11.62	27.16	3.2%
7330.15	7330.16	[O II]	(2F)	-0.411	10.90	25.53	3.2%
7530.49	7530.54	[Cl IV]	(1F)	-0.430	0.47	1.16	
7592.89	7592.74	He II	(6)	-0.436	0.71	1.77	22.7%
7712.99		line?		-0.448	0.07	0.18	
7726.14	7726?	[S I]	(3F)	-0.449	0.12	0.29	
7751.08	7751.12	[Ar III]	(1F)	-0.451	4.23	10.76	35.3%
8045.62	8046.10	[Cl IV]	(1F)	-0.477	0.82	2.20	
8196.54	8197?	C III?		-0.489	0.37	1.01	
	8236.77	He II	(6)				
8236.67	8236.90	H I	P47	-0.492	1.06	2.95	
8292.07	8292.31	H I	P29	-0.497	0.08	0.23	
8299.24	8298.84	H I	P28	-0.497	0.15	0.41	
8342.30	8342.37	He I	*	-0.501	0.23	0.67	
8353.96		?		-0.503	0.09	0.25	

Table 3 – *continued*

$\lambda_{obs'd}$ (1)	λ_{lab} (2)	Element (3)	Mult. (4)	k_λ (5)	I(Ham) (6)	F(Ham) (7)	RMS (8)
	8359.66	He I	*				
8359.23	8359.01	H I	P22	-0.504	0.22	0.61	
8361.69	8361.69	He I	*	-0.504	0.17	0.47	
8374.56	8374.48	H I	P21	-0.506	0.18	0.50	56.6%
8392.29	8392.40	H I	P20	-0.509	0.15	0.43	
8413.21	8413.32	H I	P19	-0.512	0.21	0.61	
8437.94	8437.96	H I	P18	-0.516	0.14	0.40	
8467.12	8467.26	H I	P17	-0.521	0.50	1.47	
8502.73	8502.49	H I	P16	-0.526	0.33	0.97	35.3%
8545.42	8545.38	H I	P15	-0.532	0.50	1.49	
8578.82	8578.70	[Cl II]	(1F)	-0.537	0.25	0.77	10.6%
8598.39	8598.39	H I	P14	-0.540	0.53	1.62	9.7%
8665.00	8665.02	H I	P13	-0.550	0.72	2.24	
8750.49	8750.48	H I	P12	-0.562	1.06	3.40	
8862.88	8862.79	H I	P11	-0.578	1.07	3.54	32.5%
9014.80	9014.91	H I	P10	-0.599	1.33	4.61	
9068.81	9068.90	[S III]	(1F)	-0.606	23.76	83.37	6.5%
9229.03	9229.02	H I	P9	-0.612	2.39	8.51	
9531.13	9531.00	[S III]**	(1F)	-0.620	51.67	186.64	5.9%
9546.42	9545.97	H I**	P8	-0.620	0.86	3.09	58.3%
9850.02	9850.24	[C I]	(1F)	-0.627	0.34	1.25	
10049.60	10049.38	H I	P7	-0.632	2.42	8.95	54.5%
10123.61	10123.61	He II	(2)	-0.633	3.25	12.08	

*Identification of He I from Osterbrock et al. (1992).
**Lines affected by atmosphere.
?Unlikely or doubtful identification.

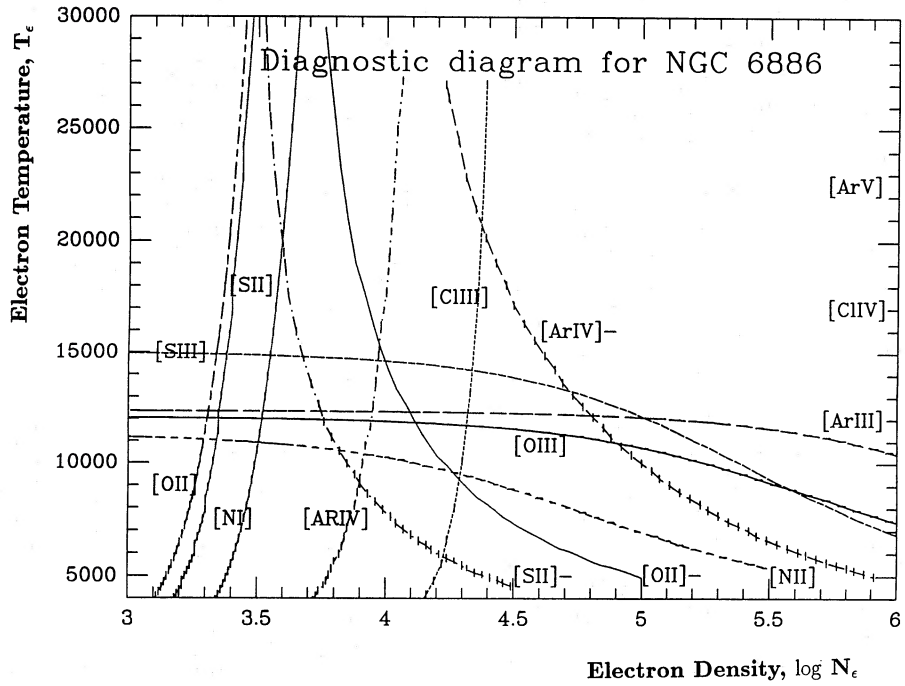

Figure 2. Diagnostic diagram for NGC 6886 (Hamilton data). The ratios of nebular-type transitions in p^3 configurations of [N I], [Cl III] and [Ar IV] depend mostly on N_e, but the auroral/nebular type transitions in O^+ and S^+, denoted as [O II]- and [S II]- respectively, are sensitive to both T_e and N_e. The well-known auroral/nebular-type transitions such as $\lambda 4363/\lambda 5007$ in [O III] or $\lambda 5755/\lambda 6584$ in [N II] depend primarily on T_e until N_e exceeds 10 000 cm^{-3}.

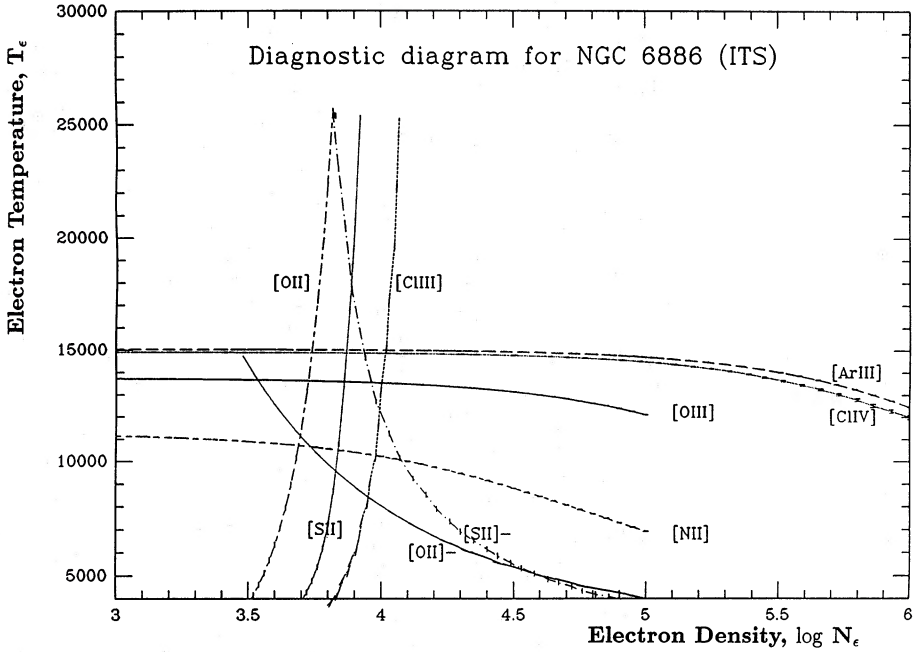

Figure 3. Diagnostic diagram for NGC 6886 (ITS). The temperature indicated by [Cl IV] seems too low, probably due to the error in [Cl IV]λ5323.

is less efficient than in the red region and, for the near-UV, improved ITS data were obtained by Likkel & Aller. Consequently, longer blue-region exposures with the Hamilton echelle would be desirable. The density indicated by [O II]λ3729/λ3726 from photographic photometry and [S II]λ6717/λ6730 ($N_e \sim 5600$ cm^{-3}) in Fig. 3 is more consistent with those obtained by others than with the results from the Hamilton echelle spectrograph. Subtraction of 'drip' from Hα on λ6717 may have been incomplete. The discordances between the Hamilton and the ITS may be partly attributed, not only to different spectral resolutions, but also to differing aperture (slot) sizes and positioning of the slot on the nebular image. The image did not rotate with the ITS. The usual observational errors enter as well.

The diagnostics from the ITS data indicate that the bulk of the optical radiation arises from high-excitation-temperature gases ($T_e = 12\,000$ K, $N_e = 5000$–$10\,000$ cm^{-3}), but the totality of the data suggest that NGC 6886 may actually be a complicated object. In many investigations mean values of diagnostic parameters have been chosen for all ions, but here we try a refinement by making use of model predictions for the T_e (see Section 4). The determination of an ionic concentration is less sensitive to the density fluctuations than to the temperature fluctuations; we adopted a mean $N_e = 7000$ cm^{-3} for the nebular electron density. Table 4 gives the fractional ionic concentrations for NGC 6886. The first three columns give, successively, the ions, the lines that are used, and their intensities from our Hamilton echelle, ITS, *IUE* and IR data, corrected for interstellar extinction. Then we list the electron temperatures, chosen on the basis of the model described in the next section. Column (5) lists the ionic concentrations in terms of $N(H^+)$, while the last column gives the ratio of the sum of the observed ionic concentrations, to which an ionization correction factor (ICF) derived from a model is to be applied. Note that model T_es tend to be higher than those found from Hamilton data

Table 4. Fractional ionic concentration for NGC 6886.

Ion	Lines	I_{corr}	T_e	$\frac{N(i)}{N(H^+)}$	$\Sigma\frac{N(i)}{N(H^+)}$
He I	4471	3.22	14500.	0.0685	
He I	5876	9.41	14500.	0.0527	
He II	4686	46.22	16500.	0.0418	
He II	5412	3.14	16500.	0.0208	0.0919
C III	1907,1909	[934.0]	14000.	2.51E-04	
C IV	1549,1551	[603.0]	16000.	4.34E-05	2.95E-04
N I	5198,5200	1.09	11000.	5.70E-07	
N II	6548/84,5755	290.75	12000.	2.83E-05	
N III	1747-1754	[53.0]	14000.	6.26E-05	
N IV	1483-1487	[49.9]	16000.	2.65E-05	
N V	1239,1243	[64.2]	18000.	8.70E-06	1.26E-04
O I	6300,6363	15.27	12000.	9.97E-06	
O II	3727,7319/30	123.93	12500.	3.56E-05	
O III	4959,5007	2252?(1839)	14000.	2.35(1.92)E-4	
O III	4363	18.42	14000.	1.58E-04	
O III	1658,1666	[41.4]	14000.	1.64E-04	
O IV	1403-1413	[63.2]	15000.	8.25E-04	2.89E-04
Ne III	3868,3967	198.47	13500.	4.33E-05	
Ne IV	2423,2425	[150.0]	15500.	3.19E-05	
Ne IV	4724-4726	1.19	15500.	2.89E-05	
Ne IV	1602	[38.10]	15500.	4.91E-4$^{\times}$	
Ne V	3347,3426	(113.80)	17000.	1.49E-05	8.86E-05
Na IV	3241,3362	(1.32)	15000.	4.22E-07	4.22E-07
Mg II	2797,2804	[21.7]	12000.	4.06E-07	4.06E-07
Si III	1884,1892	[32.0]	15000.	3.24E-06	3.24E-06
S II	6717,6731	18.16	12500.	5.37E-07	
S II	4068,4076	6.59	12500.	4.48E-07	
S III	6312,9069,9535	78.17	13000.	1.70E-06	
S IV	10.5μm	(58)	15000.	1.67E-06	3.86E-06
Cl II	8580	0.25	12500.	1.64E-08	
Cl III	5517,5537	1.52	13000.	5.58E-08	
Cl IV	7530,8045	1.29	14000.	4.28E-08	
Cl IV	5323	0.10	14000.	7.17E-8$^{\times}$	1.29E-07
Ar III	7135,7751,51	30.84	14000.	1.02E-06	
Ar IV	4711,4740	13.58	15000.	4.59E-07	
Ar IV	7265/40	0.89	15000.	1.42E-6$^{\times}$	
Ar V	6435,7005	3.00	16000.	1.28E-07	1.52E-06
K IV	6103	0.32	15000.	3.43E-08	
K V	4163	(0.14)	16000.	1.83E-08	5.26E-08
Ca V	5309	0.18	15500.	4.13E-08	4.13E-08

when a comparison can be made; T_e(O III) ≃ 14 000 K from the model but ~12 000 K (Ham) in Fig. 2 to ~14 000 K (ITS) in Fig. 3 from the diagnostic diagram.

4 THEORETICAL MODEL

The high-excitation nebula NGC 6886 is catalogued as having a very faint and very hot PPN (m_v = 19.5, Pottasch 1981). Due to the superior seeing on Mauna Kea (~0.8 arcsec), Heap et al. (1991) were able to detect the central star; the visual magnitude is m_v = 18.76, and accordingly the intrinsic visual magnitude m_{v_0} = 16.90, using their $E(B-V)$ = 0.30 and corresponding total extinction, A_v, here taken as $3.1E(B-V)$. The Zanstra and Ambartsumian temperatures derived by them were T_z(H I) = 210 000 K and T_z(He II) = 174 000 K and T(He II/H I) = 149 000 K, while much lower Zanstra temperatures were obtained by other studies, e.g, T_z(H I) = 118 000 K and T_z(He II) = 120 000 K by Pottasch (1984). Heap et al. estimate the PNN mass to be 0.65 $M_\odot$ at an assumed distance of 1.7 kpc.

The distance to NGC 6886 seems poorly determined by statistical methods, ranging from a large value of 5.7 kpc (Cahn & Kaler 1971) to 0.38 kpc (Phillips & Pottasch 1984). We carried out a number of trials, assuming different distances of 1.7 kpc (by a kinematic method, Gathier, Pottasch & Goss 1986) and 2.0 kpc (by an extinction method, Pottasch 1983). We adopted d = 2000 pc. We used Hubeny's non-LTE atmospheres (1988) corresponding to effective temperatures T_* = 160 000 and 150 000 K and log g = 7.5, 7.0 and 6.5. In these trials, constant H densities, N_H = 5000, 6000, 7000 and 10 000 atom cm^{-3}, were employed in an essentially spherical nebular shell.

The best results were found with N_H = 6000 atom cm^{-3}, corresponding to an average electron density in the PN, N_e ≃ 7000 electron cm^{-3}. The inner and outer boundaries, R(in) and R(out), are 0.001 and 0.0345 pc, respectively. Thus the model nebula is basically an homogeneous shell whose outer boundary is assumed to be material-bounded (but slightly inside the Strömgren sphere). Table 5 summarizes the data for the final model. We adopted a distance of 2.0 kpc and $T_{\rm eff}$ = 150 000 K in order to account for the He II lines, but a slightly lower temperature may be preferable. We assume log g = 6.5 and R_* = 0.046 $R_\odot$; then L_* = 970 $L_\odot$. A description of the modelling procedures, including references to selected atomic parameters, may be found in Hyung (1994). We assumed that, in the radiating strata, the dust-to-gas ratio, m(dust)/m(gas) = 0.001. Except for some UV lines, e.g., C IV λλ1549/1551, the effect of such a small amount of dust is negligible.

The observed absolute Hβ flux by Heap et al. is $F(\mathrm{H}\beta) = 5.2 \times 10^{-12}$ erg cm^{-2} s^{-1} [10^{-12} is denoted as (−12) hereafter], and the absolute intrinsic flux is $F_{\rm corr}(\mathrm{H}\beta)$ = 4.2(−11) using C = 0.9. A compilation by Acker et al. (1992) gives $F(\mathrm{H}\beta)$ = 4.9(−12); then $F_{\rm corr}(\mathrm{H}\beta)$ would be 3.9(−11). For a distance range of 1.7–2.0 kpc, the model reproduces the absolute Hβ flux to within observational errors. The predicted intrinsic visual magnitude of m_{v_0} = 16.90 is consistent with the measurement by Heap et al. An alternative model with N_H = 10 000 atom cm^{-3}, R(in) = 0.001 pc and R(out) = 0.025 pc also tends to fit the observed line intensities fairly well. However, we prefer the model with N_H = 6000 atom cm^{-3} (see Section 2.2; a fairly consistent extinction coefficient, C, was found from the H Balmer and Paschen lines using a nebular physical condition with N_e = 7000 cm^{-3} and T_e = 12 000 K). The adopted abundance ratios with respect to H are as follows: He = 0.093, C = 4.30(−4), N = 1.30(−4), O = 3.05(−4), Ne = 1.62(−4), Na = 1.40(−6), Mg = 2.30(−6), Si = 1.15(−5), S = 5.25(−6), Cl = 1.40(−7) and Ar = 1.70(−6), where the number in parentheses (...) indicates the power of 10 by which the entry is to be multiplied.

Table 6 compares observed (column 3) and predicted (column 4) intensities for the final model. The predicted values pertain to the whole nebula, and we have not considered the slit size in the predictions. The current final model can therefore accommodate only the overall nebular

Table 5. Details of the final model.

Adopted distance =2000pc (see Text)

Shell: hydrogen density N_H =6000 atomscm^{-3} R(in), R(out) = 0.001, 0.0345pc
Observed <T_e>≃ 12000–13000K([OIII],[ArIII]) Predicted <T_e>≃ 14000K([OIII])

Central star
T(⋆)= 150000K, log g = 6.5 Radius = 0.046 R(⊙)
L(⋆)= 970L(⊙)
Hubeny non-LTE model (He/H=0.095)

Observed F(Hβ)≃ 3.9 × 10^{-11} ergs cm^{-2} s^{-1} (Acker et al. 1992, C = 0.9)
Predicted F(Hβ)≃ 3.8 × 10^{-11} ergs cm^{-2} s^{-1}

Assumed Abundances

He	C	N	O	Ne	S	Ar	Cl
9.30E-02	4.30E-04	1.30E-04	3.05E-04	1.62E-04	5.25E-06	1.70E-06	1.40E-07

P	Na	Ca	Mg	F	K	Si
5.00E-08	1.40E-06	2.00E-07	2.30E-06	1.00E-08	7.50E-08	1.15E-05

Table 6. Comparison of observed and predicted intensities in NGC 6886.

El Ion (1)	λ(Å) (2)	I_{obs} (3)	I_{cal} (4)	El Ion (1)	λ(Å) (2)	I_{obs} (3)	I_{cal} (4)
He I	5876	9.41(9.53)	9.11{9.78}	Ne III	3868	146.93(155)	365.65{362.96}
	6678	2.74(2.04)	2.13{2.27}		3969	51.54(44)	109.05{108.26}
	4471	3.22(3.21)	3.26{3.49}	Ne IV	2422/25	[150]	137.82{131.69}
He II	4686	46.22(44.60)	45.16{46.22}		4725/27	1.19	1.28{1.45}
	5412	3.14(3.07)	3.83{3.61}	Ne V	3347	(29.5)	31.25{33.99}
	3203	(15.50)	19.87{18.74}		3426	(84.3)	85.11{92.54}
	1640	[292.0]	334.96{316.83}				
				Mg II	2796\	[20.1]	18.81{19.72}
C II	2325\	-	14.29{14.90}		2806/	-	9.48{9.94}
	2328/	<[193]	142.65{148.79}				
	4267	0.43(0.36)	0.23{0.22}	S II	4068	4.86(4.5)	3.74{4.77}
C III	1907\	-	460.59{430.23}		4076	1.73(1.7)	1.28{1.56}
	1909/	[934]	352.10{358.73}		6717	5.92(3.67)	4.64{4.03}
C IV	1548\	-	595.68{645.74}		6731	12.24(7.2)	8.31{8.05}
	1551/	[603]	300.77{326.00}	S III	6312	2.74(2.4)	2.54{2.4}
					9069	23.76(31.8)	30.51{29.15}
N II	6584	215.24(177.0)	211.229{220.47}		9531	51.67[a](91.9)	74.33{91.9}
	6548	71.02(51.2)	72.93{76.10}	SIV	10.5μm	(89-58)[1]	64.98{56.01}
	5755	4.49(3.57)	6.34{6.94}				
N III	1747-52	[53.0]	53.05{51.94}	Ca V	5309	0.18(0.06)	0.16{0.15}
	2754	-	5.51{5.23}				
N IV	1483/86	[49.9]	49.01{53.74}	Cl II	8580	0.25(0.42)	0.30{0.34}
N V	1239/42	[64.1]	46.61{54.52}	Cl III	5517	0.43(0.41)	0.50{0.38}
					5538	1.09(0.76)	0.76{0.74}
O I	6300	10.76(10.2)	2.63{4.75}	Cl IV	7530	0.47(0.35)	0.33{0.32}
	6363	4.25(3.2)	0.84{1.51}		8046	0.82(0.66)	0.76{0.75}
O II	3726\	61.38(107.0)	109.58{94.75}				
	3729/	40.03(52.5)	48.23{38.42}	Ar III	5193	0.28(0.32)	0.22{0.22}
	7321/2\	11.62(15.30)	11.62{14.14}		7136	26.33(18.50)	17.47{17.45}
	7332/3/	10.90(——)	9.31{11.34}		7751	4.23(4.20)	4.22{4.17}
O III	1660\	[41.4]	14.72{14.81}	Ar IV	4711	5.92(——)	6.11{5.28}
	1666/	[——]	36.12{36.34}		4740	7.66(6.90)	7.38{7.74}
	4363	18.42(22.28)	22.22{22.28}	Ar V	6435	1.11(0.76)	1.16{1.18}
	4959	537.24[7](490)	458.32{444.47}		7005	1.89(1.51)	2.48{2.53}
	5007	1715[7](1349)	1320{1280}				
O IV	1403-13	[68.2]	22.82{25.12}	K IV	6103	0.32(0.30)	0.29{0.28}
				K V	4163	(0.14)	0.10{0.10}
Si III	1883/92	[32]	32.79{30.60}				
				Na IV	3241/3361	(1.32)	{1.13}

physical states, not the detailed structure. The observed intensities enclosed in parentheses, i.e. (I_{obs}), are the ITS and other data, mostly from Tables 2(a) and (b) and as compiled by Aller & Czyzak (1979). The Hamilton data are given without parentheses. We list predicted intensities, I_{cal}, both for $N_H = 6000$ and 10 000 atom cm^{-3}, all on the scale of $I(H\beta) = 100$; the latter are indicated by { }. The Hamilton echelle and ITS observations are in general agreement. However, some lines disagree. Note that the predicted [O III] values for lines λλ4363, 4959 and 5007 fit more closely the Aller & Czyzak compilation. The size of a slit in ITS was typically 2 × 4 or 2 × 6 arcsec^2. Thus the ITS line intensities, which form the backbone of the Aller & Czyzak compilation and the *IUE* data, more closely resemble the integrated values over a whole nebula (diameter ~ 5.52 arcsec) and the final model as well, because of the relatively small nebular size. There are other possible explanations for a notable intensity discrepancy between the primarily ITS and the Hamilton data: (1) the Hamilton echelle data represent the central part of the PN, while the ITS data correspond to the flux integrated over most of the whole PN; (2) errors in the observational data; and (3) a real time variation might exist, but the evidence is unconvincing. It is likely that effect (1) is true, so we may need to construct eventually a more detailed axisymmetric nebular model to fit the observed isophotic contour map so that we can apply the slit size correctly. To justify this effort, some monochromatic isophotic and perhaps additional spectroscopic data are required.

Note that the predicted value of C IV λλ1549/1551 is too high. This might be due to the effect of dust on the UV resonance lines. The predictions for S seem much more successful than those in other PN: the Hamilton [S III]λλ9069/9531 line data are affected by atmospheric water-vapour extinction. The observed [O I]λλ6300/6363 line intensities, which presumably originate in neutral blobs, are stronger than the predicted values. The calculated and

observed intensities also disagree in [Ne III]λλ3868/3969 and C II λ4267. It has been a long-standing problem that ionization models cannot give a satisfactory prediction of both [Ne V] and [Ne III] at the same time using a currently available standard model atmosphere energy distribution (Middlemass 1990; Hyung 1994): Adam & Köppen (1985) proposed that the stellar wind of the PNN could affect the ionizing continuum absorbed by the nebula. The atomic data in these lines might be in error. If we adjust the C abundance to fit the observed C II recombination line $4f\,^2F^0-3d\,^2D\lambda4267$, the C abundance should be increased by a factor of 2. The C^{2+} abundances derived from the C II λ4267 are generally higher than those deduced from the collisionally excited C III]λ1908 (Barker 1991, and references therein; see also Peimbert, Storey & Torres-Peimbert 1993 and Hyung, Aller & Feibelman 1994 for similar discordances found in other permitted lines of O II, C III, N II and N III). Studies of recombination employing the whole body of nebular data could shed light on this problem.

To find the chemical abundances using the fractional ionic concentration in Table 4, it is necessary to calculate from the model ICFs for the ionization stages that are not observed. Alternatively, one can directly adopt the derived abundances with which the model gives the best fit to the observed fluxes. Table 7 gives the final abundances. Comparing the ICF method and the model results, we find big discordances for Ne and Si. ICF factors for Si, and also Mg, are large and uncertain. The values of Δ express the logarithmic discordance, i.e. log N(ICF) − log N(model). The last column of the table gives the solar composition (Grevesse & Anders 1989).

If we compare the mean of ICF and model calculations, we find the following results: C, N and Ne have approximately solar values; O, S, Cl and Ar are depleted by factors ranging from 2 to 3; Na and K, and probably Mg, are reduced by a factor of around 1.5, while Ca is depleted by about a factor of 8. We can raise the O abundance up to the solar value by postulating T_ε fluctuations (Peimbert 1967); then the C/H, N/H and Ne/H ratios would lie substantially above the corresponding solar values, and this seems unlikely. The Peimbert's temperature fluctuation parameter would need to be $t^2\sqrt{0.1}$ to raise the O abundance up to the solar value, which is rather high.

Table 7. Relative chemical abundances of NGC 6886.

Element	$\Sigma\frac{N(i)}{N(H^+)}$	ICF	ICF Method	Model	Δ	Sun*
He	0.0919	-	0.092	0.093	—	0.098
C	2.95E-4	1.404	4.14E-4	4.30E-4	-0.02	3.6E-4
N	1.26E-4	1.034	1.30E-4	1.30E-4	0.00	1.1E-4
O	2.89E-4	1.087	3.14E-4	3.05E-4	0.01	8.5E-4
Ne	8.86E-5	1.094	1.00E-4	1.62E-4	-0.21	1.2E-4
Na	4.22E-7	3.331	1.40E-6	1.40E-6	0.00	2.1E-6
Mg	4.06E-7	7.194	2.92E-6	2.30E-6	0.10	3.6E-5
Si	3.24E-6	6.993	2.26E-5	1.15E-5	0.29	1.6E-5
S	3.86E-6	1.220	4.71E-6	5.25E-6	-0.04	1.6E-5
Cl	1.29E-7	1.536	1.98E-7	1.40E-7	0.15	3.2E-7
Ar	1.52E-6	1.199	1.82E-6	1.70E-6	0.03	3.6E-6
K	5.26E-8	1.443	7.59E-8	7.50E-8	0.01	1.3E-7
Ca	4.13E-8	4.878	2.01E-7	2.00E-7	0.00	1.6E-6

*Solar abundances by Grevesse & Anders (1989)

The progenitor star may have been an object in which C, N and Ne had essentially solar abundances, while heavier elements such as S, Cl and Ar were less plentiful as noted above. The depletion of O remains puzzling. It cannot be removed without increasing abundances of elements in the first row of the Periodic Table. O may have been depleted in the progenitor star by hot bottom burning. The predicted visual magnitude and the overall nebular line intensities are generally in accord with those observed. Thus, if the assumed distance to the PN is correct, the employed PNN temperature (and surface gravity) and luminosity should give us a PNN mass. The Schönberner (1981) track gives a mass of about 0.598 $M_\odot$, which is smaller than the value of 0.65 $M_\odot$ suggested by Heap et al. (1991). An age of about 9400 yr is implied. We must emphasize that, until the nebular distance is accurately determined, conclusions about stellar evolution remain somewhat speculative.

ACKNOWLEDGMENTS

We thank Dr T. Barker for reviewing our paper, and for his helpful suggestion to add a fuller discussion on the disagreement between theory and observation in Table 6. The ground-based observational aspects of this programme were supported in part by a Grant from the Research Committee of UCLA, and in part by National Science Foundation Grant AST 90-1433 to UCLA, while the UV observations with the *International Ultraviolet Explorer* satellite were supported in part by National Aeronautics and Space Administration Grant NAG 5-1207 ADF to UCLA. We are indebted to Dr Likkel, who measured the near-UV lines in connection with an investigation of the Bowen fluorescent mechanism (Likkel & Aller 1986). For the image-tube scanner observations we acknowledge support by National Science Foundation Grant AST 83-12384. The Hamilton spectrograph was made possible by a gift to Lick Observatory from Ms Clara-Becle Hamilton, while a NSF core grant AST 83-20396 to Lick Observatory enabled the development of the necessary software to operate the equipment.

REFERENCES

Acker A., Ochsenbein F., Stenholm B., Tylenda R., Marcout J., Schohn C., 1992, Strasbourg - ESO Catalogue of Galactic Planetary Nebulae. European Southern Observatory, Garching bei München
Adam J., Köppen J., 1985, A&A, 142, 461
Aller L. H., 1974, in Lange K. R., ed., Astrophysical Formulae. Springer, Berlin, p. 110
Aller L. H., Czyzak S. J., 1979, Ap&SS, 62, 397
Aller L. H., Keyes C. D., 1981, in Chapman R. D., ed., The Universe at Ultraviolet Wavelengths. NASA Conf. Publ. 2171, p. 649
Barker T., 1991, ApJ, 371, 217
Beck S. C., Lacy J. H., Townes C. H., Aller L. H., Geballe T. R., Baas F., 1981, ApJ, 249, 592
Cahn J. H., Kaler J. B., 1971, ApJS, 22, 319
Cahn J. H., Kaler J. B., Stanghellini L., 1992, A&AS, 94, 399
Che A., Köppen J., 1983, A&A, 118, 107
Gathier R., Pottasch S. R., Goss W. M., 1986, A&A, 157, 191
Grevesse N., Anders E., 1989, in Waddington J., ed., Cosmic Abundances in Matter. American Institute of Physics, New York, p. 1

Heap S. R., Corcoran M., Hintzen P., Smith E., 1991, The Properties of the Hottest Central Stars of Planetary Nebulae. NASA/ Goddard Space Flight Center Preprint
Hubeny I., 1988, Comput. Phys. Comm., 52, 103
Hummer D. G., Storey P. J., 1987, MNRAS, 224, 801
Hyung S., 1994, ApJS, 90, 119
Hyung S., Aller L. H., Feibelman W. A., 1994, ApJS, 93, 465
Likkel L., Aller L. H., 1986, ApJ, 301, 825
Middlemass D., 1990, MNRAS, 244, 294
Moore C. E., 1972, A Multiplet Table of Astrophysical Interest, Natl. Bur. Stand. No. 40
Osterbrock C. R., Tran H. D., Veilleux S., 1992, ApJ, 389, 305
Peimbert M., 1967, ApJ, 150, 825
Peimbert M., Storey P. J., Torres-Peimbert S., 1993, ApJ, 414, 626
Phillips J. P., Pottasch S. R., 1984, A&A, 130, 91
Pottasch S. R., 1981, A&A, 94, L13
Pottasch S. R., 1983, in Flower R. D., ed., Proc. IAU Symp. 103, Planetary Nebulae. Reidel, Dordrecht, p. 391
Pottasch S. R., 1984, Planetary Nebulae. Reidel, Dordrecht, p. 298
Rowlands N., Houck J. R., Herter T., Gull G. E., Skrutskie M. F. N., 1989, ApJ, 341, 901
Sabbadin F., 1984, A&AS, 58, 273
Schönberner B., 1981, A&A, 103, 119
Seaton M. J., 1979, MNRAS, 187, 73P
Taylor A. R., Gussie G. T., Pottasch S. R., 1990, ApJ, 351, 515
Weinberger R., 1989, A&AS, 78, 301